

Tunable bandgaps and excitons in doped semiconducting carbon nanotubes made possible by acoustic plasmons

Catalin D. Spataru^{*1} and François Léonard¹

¹*Sandia National Laboratories, Livermore, CA 94551, USA*

Doping of semiconductors is essential in modern electronic and photonic devices. While doping is well understood in bulk semiconductors, the advent of carbon nanotubes and nanowires for nanoelectronic and nanophotonic applications raises some key questions about the role and impact of doping at low dimensionality. Here we show that for semiconducting carbon nanotubes, bandgaps and exciton binding energies can be dramatically reduced upon experimentally relevant doping, and can be tuned gradually over a broad range of energies in contrast to higher dimensional systems. The later feature is made possible by a novel mechanism involving strong dynamical screening effects mediated by acoustic plasmons.

Nanomaterials have been lauded for their promise in electronic and photonic applications [1]. Quite often, the imagined nanodevices rely on analogies with those based on bulk semiconductors. However, the true potential of nanomaterials lies in the exploitation of their unique properties to realize entirely new device concepts. In particular, approaches for externally controlling their electronic and optical properties would enable new strategies for device design.

Here we propose that such control is possible in carbon nanotubes (CNTs) through electrostatic doping. We find that quasiparticle (QP) band gaps and exciton binding energies can be reduced dramatically by hundreds of meVs upon doping, and yet prominent optical absorption features shift by relatively small amounts. Furthermore, we show that doping has a unique influence on CNT exciton properties: in contrast to bulk excitons, bound excitons in semiconducting CNTs are not quenched by doping and their binding energy can be tuned gradually even at very high doping. These features arise due to the presence of acoustic plasmons and their impact on dynamical screening.

We utilize a many-body *ab initio* approach [2–4] to calculate the electronic and optical properties of electrostatically doped semiconducting CNTs. We focus on the semiconducting (10,0) CNT, with diameter $D = 0.78$ nm, and perform *ab initio* calculations [5] at zero doping and for a free carrier concentration $\rho = 0.6$ holes/nm. We use the GW approach [2] to obtain QP properties near the Γ point and solve the Bethe-Salpeter (BS) equation for the excitonic effects [3]. Applying this approach to doped CNTs necessitates careful consideration because of the presence of acoustic plasmons, a unique feature of low-dimensionality materials [6, 7].

Indeed, in quasi-1D systems such as CNTs, electron gas and tight-binding models predict “acoustic” plasmons, whose energies approach zero in the long wavelength limit $\tilde{\omega}_{ap}(q \rightarrow 0) \propto q\sqrt{\rho \log(|q|D/2)}$. Our *ab initio* calculations also reveal these plasmons in doped CNTs [8]: Fig. 1a shows the inverse dielectric function $\epsilon_{00}^{-1}(q = 0.35 \text{ nm}^{-1}, E)$ of the (10,0) CNT at $\rho =$

0.6 holes/nm. The peak in $\text{Im}\epsilon^{-1}$ signals a low-energy plasmon, which gives rise to a transition in $\text{Re}\epsilon^{-1}$ between a very small value at zero energy and a value close to 1 above the plasmon energy, *i.e.* a transition between metallic-like and semiconducting-like screening [9]. These acoustic plasmons span a broad range of energies, as seen in Fig. 1b, and dynamical screening effects due to them are very important for both QPs and excitons and cannot be neglected or simply integrated out.

To include these dynamical screening effects during the GW calculations we modify methods previously applied in the context of doped bulk semiconductors [10]. In the undoped case, optical plasmons in CNTs have energies above ~ 5 eV [11], and their contributions is taken into account through the Generalized Plasmon Pole (GPP) approximation [2]. In the doped case, GPP alone does not describe satisfactorily dynamical effects from acoustic plasmons and the screening is evaluated instead from $\epsilon^{-1} = \epsilon_{int}^{-1} + \delta\epsilon^{-1}$, where ϵ_{int} is the dielectric function of the intrinsic semiconductor for which we make use of the GPP approximation and $\delta\epsilon^{-1}$ is obtained within the Random Phase Approximation.

Dynamical effects are included in the BS calculations by an *effective* dielectric screening $\tilde{\epsilon}$ that depends self-consistently on the binding energy E_B of the exciton [12]. Taking advantage of the fact that for the excitons considered here most of the corresponding electron-hole transitions have energies close to the onset of the electron-hole continuum, and neglecting finite lifetime effects, one can write to first order in dynamical effects [13]:

$$\tilde{\epsilon}^{-1}(q; E_B) \approx \epsilon^{-1}(q, 0) - \frac{2E_B}{\pi} \int_0^\infty d\omega \frac{\text{Im} \epsilon^{-1}(q, \omega)}{\omega(\omega + E_B)}. \quad (1)$$

When low-energy plasmons are absent, the commonly used static approximation is obtained by retaining the first term on the *r.h.s.* of Eq. (1). The second term captures dynamical effects due to acoustic plasmons (we neglect dynamical effects due to optical plasmons during the BS calculations in both undoped and doped cases). Smaller, higher order corrections in dynamical effects (not shown in Eq. (1)) due to acoustic plasmons are

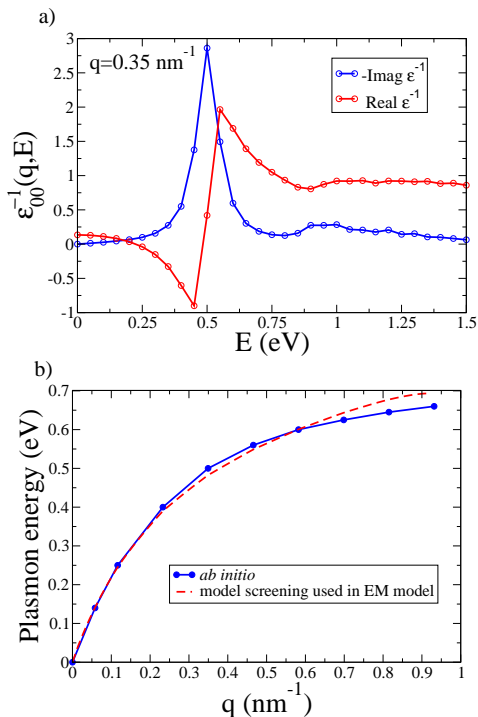


FIG. 1: Dielectric properties of the (10,0) doped CNT. a) Real and imaginary parts of the inverse dielectric function as a function of energy calculated *ab initio* for a fixed wave-vector $q = 0.35 \text{ nm}^{-1}$. The subscripts on ϵ^{-1} imply their evaluation at $\vec{G} = \vec{G}' = 0$. b) Plasmon dispersion relation calculated *ab initio* and within the model screening used in the effective mass model. Doping level $\rho = 0.6$ holes/nm.

included as well in our calculations.

Fig. 2 shows a sketch of the calculated QP bands and exciton level associated with the lowest prominent optical transition (E_{11}), before and after doping, where the energy scale has been preserved between the two cases. The quantities of interest are the bandgap E_g^{11} and the exciton binding energy E_B^{11} . It is clear from this figure that the bandgaps and exciton binding energies are significantly reduced by doping. In fact, at this doping ($\rho = 0.6$ holes/nm), E_g^{11} is reduced by 800 meV, while E_B^{11} is reduced by 590 meV. Both of these changes are large by any measure; in particular we estimate that band gap renormalization (BGR) is about an order of magnitude larger than in typical bulk semiconductors at the same doping [14]. The QP bands and exciton level associated with the second lowest prominent optical transition (E_{22} , not shown in Fig. 2) also suffer from a significant bandgap reduction of 130 meV [15], and a decrease of the exciton binding energy by 240 meV. Moreover, doping leads to an important 40% reduction in the effective mass at the valence band maximum for E_{11} .

The excitonic effects are presented in more detail in Fig. 3, where the optical absorption spectra for light polarized along the tube axis is calculated in two ways. The

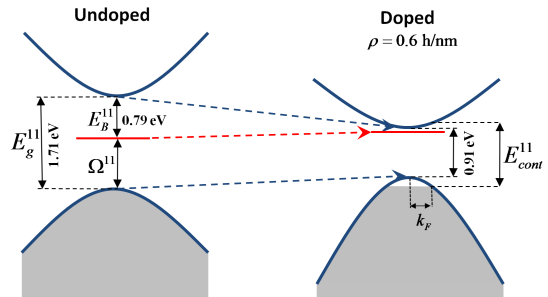


FIG. 2: Illustration of bandgap and exciton renormalization in the (10,0) CNT. The blue lines indicate the E_{11} valence and conduction bands, and the bound exciton is indicated by a red line. Occupied electronic states are indicated by the shaded areas, and the highest occupied energy levels have been aligned between the doped and undoped cases. The different band curvatures represent the change in effective mass upon doping.

blue lines are obtained neglecting the electron-hole interaction, with the corresponding onset energies indicating the electron-hole continua. The red lines show the correct absorption spectra obtained with the electron-hole interaction included. As each bound exciton requires a separate self-consistent calculation in the doped case, we have focused on the lowest energy bright exciton associated with each of the E_{11} and E_{22} continua.

In the undoped case, the E_{11} and E_{22} excitons show very large binding energies: $E_B^{11}(\rho = 0) = 0.79 \text{ eV}$ and $E_B^{22}(\rho = 0) = 1.00 \text{ eV}$. As discussed above, upon doping, a dramatic change in excitonic properties occurs. As seen in Fig. 3b, E_B^{11} suffers a decrease of $\sim 0.6 \text{ eV}$ to $E_B^{11}(\rho = 0.6 \text{ holes/nm}) = 0.20 \text{ eV}$, while the corresponding E_B^{22} renormalization is 0.24 eV (see Fig. 3d). While both the E_{11} and E_{22} excitons are affected by the change in dielectric screening, the E_{11} exciton renormalizes more because it is affected by the bleaching of transitions. We also note from Fig. 3b a six-fold reduction in the oscillator strength of the E_{11} exciton, in good accord with recent photo-luminescence measurements [16] which assigned a factor of five in the drop of the E_{11} exciton radiative decay rate of a 1.4 nm diameter CNT [for an estimated maximum doping $\rho_{\text{max}}^{\text{exp}} \approx 0.16 \text{ holes(electrons)/nm}$].

Our *ab initio* results suggest large changes in bandgap and exciton properties upon doping [17]. This could lead, for example, to engineering of CNT optoelectronic devices by electrostatic control; but taking advantage of these new features requires robust control of doping-induced properties. Because our many-body *ab initio* calculations are extremely demanding, exploring the tailoring over a broad range of doping is not possible. Therefore, we developed a compact model for excitons in doped CNTs based on an effective mass (EM) approach [18].

Our EM model seeks to describe the binding energy

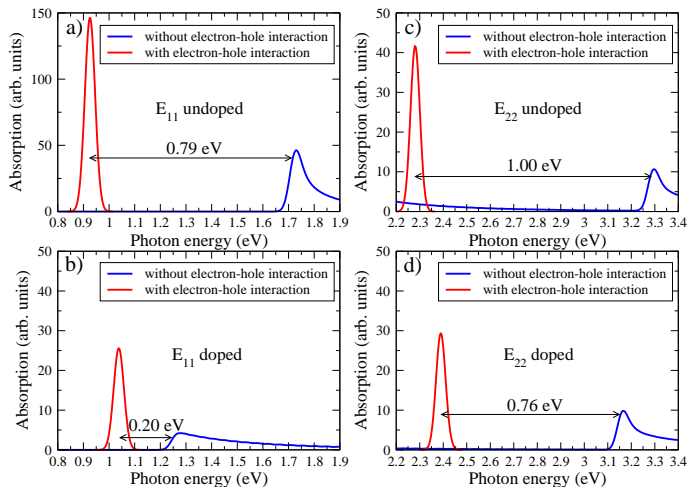


FIG. 3: Impact of doping on the electronic and optical properties of the (10,0) CNT. a,b) Optical absorption spectra near the E_{11} transition with (red) and without (blue) the electron-hole interaction. a) Before doping. b) After doping with 0.6 holes/nm. c,d) Optical absorption spectra near the E_{22} transition c) Before doping. d) After doping with 0.6 holes/nm. Arrows indicate exciton binding energies. Optical spectra are broadened by a 20 meV Lorentzian.

and envelope function of excitons in CNTs taking advantage of their large spatial extent along the tube axis relative to inter-atomic distances. The effective interaction between the electron and hole composing an exciton depends on $\tilde{\varepsilon}$ via [see Eq. (1)] the dielectric function $\varepsilon = 1 - vP$, where P is the irreducible polarizability. Our EM approximation assumes that $P(z, z', \rho, \rho', \varphi, \varphi')$ is localized on a cylindrical tubule with radius R , and that local field effects along the tube axis can be neglected. Noting that only the $L=0$ component of the angular momentum L is relevant for screening effects in excitons composed of electron-hole transitions between bands of same L , one replaces $P(z, z', \rho, \rho', L=0)$ with $\hat{P}(z - z', R, L=0)$. Relevant dynamic effects are included via $\hat{P}(\omega) \approx \hat{P}^{free}(\omega) + \hat{P}^{int}(\omega=0)$, where \hat{P}^{free} describes intraband transitions within parabolic band approximation [6], and \hat{P}^{int} represents the interband transitions for the intrinsic semiconductor. (We keep transitions from the top of valence band to conduction states as we found that they make very small contributions.) \hat{P}^{int} is extracted from *ab initio* calculations for the intrinsic polarizability (P^{int}) by imposing that \hat{P}^{int} and P^{int} yield the same average along the radial direction over one unit cell. In Fourier space this reads: $\hat{P}_{L=0}^{int}(\mathbf{q}) = \frac{A_{uc}}{\pi D} P_{\vec{G}=\vec{G}'=0}^{int}(\mathbf{q})$, where A_{uc} is the cross-sectional area of the unit cell considered in the *ab initio* case. The ability of our model -free of any adjustable parameters- in describing dynamical screening effects from acoustic plasmons is demonstrated in Fig. 1b.

Fig. 4a shows the EM results for E_B^{11} and E_B^{22} ex-

tended to carrier densities as small as $\rho \approx 1$ hole/800 nm (in terms of number of holes per atom, this corresponds to $10^{17} - 10^{18}$ holes/cm³ in typical bulk semiconductors, *i.e.*, approximately the degenerate limit). Comparison with *ab initio* results illustrates the high accuracy of our EM model. Fig. 4b shows that with good approximation, $\delta E_B^{22} \equiv E_B^{22}(\rho) - E_B^{22}(0) \propto \sqrt{\rho}$, which we found to be a signature of acoustic plasmons. A similar trend is found for δE_B^{11} , where deviations from the $\sqrt{\rho}$ behavior are more pronounced due to bleaching of transitions. More importantly, the mild dependence on doping should be contrasted to that in higher dimensional semiconductors where, at equivalent doping levels, excitons are either quenched [19] or the dependence on doping is exponential [20], giving poor control over optical properties.

The large change in exciton binding energy combined with the mild dependence on doping implies that excitonic properties in CNTs can be efficiently controlled through doping. The origin of this feature lies in the presence of acoustic plasmons. To emphasize this point, Fig. 4b also shows EM results for exciton binding energies within the static approximation, *i.e.* without proper inclusion of dynamical effects due to acoustic plasmons. In this case, binding energies drop exponentially with doping, much like is observed in two-dimensional materials [20]; moreover, the E_{11} exciton gets quenched beyond $\rho \approx 1$ hole/15 nm. The importance of acoustic plasmons is readily seen within our model and from Eq. (1), which can be shown to yield: $\tilde{\varepsilon}^{-1}(q; E_B) \approx \varepsilon^{-1}(q, 0) + \frac{E_B}{\tilde{\omega}_{ap}(q) + E_B} [\varepsilon_{int}^{-1}(q, 0) - \varepsilon^{-1}(q, 0)]$. For long wavelengths where $\tilde{\omega}_{ap}(q) \ll E_B$, one has $\tilde{\varepsilon}(q; E_B) \approx \varepsilon_{int}(q, 0)$, as opposed to the static approximation result $\tilde{\varepsilon}(q; E_B) \approx \varepsilon(q, 0)$. The difference between these two values can be orders of magnitude depending on q .

We obtain the QP fundamental bandgap versus doping using our exciton EM model and our many-body *ab initio* results for optical properties. Indeed, we can write $E_g^{11} = E_B^{11} + \Omega^{11} - \Delta E_F^{11}$ where Ω^{11} is the exciton excitation energy and $\Delta E_F^{11} \equiv E_{cont}^{11} - E_g^{11}$ (see Fig. 2). We calculate the doping dependence of ΔE_F^{11} from $\Delta E_F^{11} \cong k_F^2/2\mu^*$, with the reduced exciton mass μ^* obtained at various doping levels by interpolating the values from many-body *ab initio* calculations at $\rho = 0$ and $\rho = 0.6$ holes/nm. Furthermore, we find from our *ab initio* calculations at $\rho = 0.6$ holes/nm that Ω^{11} only increases by ~ 0.1 eV upon doping (similarly for Ω^{22}), a result of cancellation between self-energy corrections and excitonic effects [21]. The smallness of these shifts is in excellent agreement with measurements of the E_{33} absorption peak of a 1.4 nm diameter CNT [16], showing a red-shift of 20 meV at ρ_{max}^{exp} . Therefore, with little expected error, we assume a linear dependence of Ω^{11} on doping, and plot in Fig. 4c the fundamental bandgap versus doping; the trend indicates that BGR can also be tuned gradually over a broad energy range.

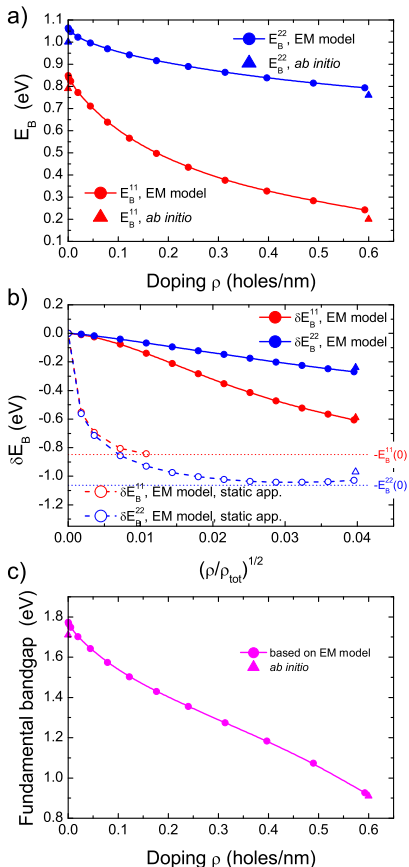


FIG. 4: Exciton binding energies and fundamental bandgap as a function of doping in the (10,0) CNT. a) Binding energies for the E_{11} and E_{22} lowest bright excitons calculated from the EM model and compared to *ab initio* results. b) Change in exciton binding energies, $\delta E_B^S \equiv E_B^S(\rho) - E_B^S(0)$, as a function of $\sqrt{\rho/\rho_{tot}}$ where ρ_{tot} is the total electron charge density, within the EM model with and without dynamical effects. The dotted lines refer to the EM model. The triangles represent *ab initio* results: within the static approximation, we find no bound exciton associated with E_{11} and $E_B^{22} \approx 30$ meV at $\rho = 0.6$ holes/nm. c) Dependence of the fundamental bandgap on doping, based on the EM model and compared to *ab initio* results.

The giant BGR discussed here is in agreement with recent experimental results [22] that combined photocurrent spectroscopy with transport measurements: for a 1.5 nm diameter CNT with QP band gap of 0.91 eV at zero doping, a BGR of 0.54 eV was deduced at a doping density of 0.7 electrons/nm.

In conclusion, we have shown that doping has a profound and unique impact on the electronic and optical properties of semiconducting CNTs, and that dynamical effects from acoustic plasmons are essential to capture these effects. Our study indicates that bandgaps and exciton binding energies in CNTs can be tuned significantly and gradually by electrostatic doping, establishing a new framework for the understanding and design

of CNT-based devices. We expect that similar control will be possible in a broad range of nanomaterials.

Sandia is a multiprogram laboratory operated by Sandia Corporation, a Lockheed Martin Company, for the United States Department of Energy's National Nuclear Security Administration under Contract DE-AC04-94AL85000. Work supported by the Lockheed Martin Shared Vision program.

* Corresponding author. E-mail: cdspata@sandia.gov

-
- [1] P. Avouris, Z. Chen, and V. Perebeinos, *Nature Nanotech.* **2**, 605 (2007); W. Lu and C.M. Lieber, *Nature Mater.* **6**, 841 (2007); P. Pauzauskie and P. Yang, *Materials Today* **9**, 36 (2006); X. Wang et al., *Phys. Rev. Lett.* **100**, 206803 (2008); I.V. Bondarev, L.M. Woods and K. Tatur, *Phys. Rev. B*, **80**, 085407 (2009).
 - [2] M.S. Hybertsen and S.G. Louie, *Phys. Rev. B* **34**, 5390 (1986).
 - [3] M. Rohlfing and S.G. Louie, *Phys. Rev. B* **62**, 4927 (2000).
 - [4] C.D. Spataru et al., *Phys. Rev. Lett.* **92**, 077402 (2004).
 - [5] Ground-state properties are obtained within Density Functional Theory in Local Density Approximation using *ab initio* pseudopotentials in a plane-wave basis. The 1D Brillouin zone is sampled by at least 128 \mathbf{k} -points (up to 512 \mathbf{k} -points during the *ab initio* excited state calculations).
 - [6] G.Y. Hu and R.F. O'Connell, *J. Phys.: Condens. Matter* **2**, 9381 (1990); O. Sato et al., *Phys. Rev. B* **48**, 1947 (1993).
 - [7] M.F. Lin and F.L. Shyu, *Physica B* **292**, 117 (2000).
 - [8] To capture this acoustic character, it is critical to truncate periodic image interactions between tubes; see S. Ismail-Beigi, *Phys. Rev. B* **73**, 233103 (2006).
 - [9] C.D. Spataru et al., *Appl. Phys. A* **78**, 1129 (2004); F. Léonard and J. Tersoff, *Appl. Phys. Lett.* **81**, 4835 (2002).
 - [10] A. Oschlies, R.W. Godby, and R.J. Needs, *Phys. Rev. B* **51**, 1527 (1995).
 - [11] C. Kramberger et al., *Phys. Rev. Lett.* **100**, 196803 (2008).
 - [12] G. Strinati, *Phys. Rev. Lett.* **49**, 1519 (1982); *Phys. Rev. B* **29**, 5718 (1984).
 - [13] We stress that $\tilde{\epsilon}^{-1}(q; E_B) \neq \epsilon^{-1}(q, \omega = E_B)$, as an electron excited in a conduction band probes the density response of the system with a hole in the valence band [12].
 - [14] R.A. Abram, G.J. Rees, and B.L.H. Wilson, *Adv. Phys.* **27**, 799 (1978).
 - [15] Within GPP alone during GW, E_g^{11} and E_g^{22} are reduced upon doping by 890 meV and 800 meV respectively.
 - [16] M. Steiner et al., *Nano Lett.* **9**, 3477 (2009).
 - [17] Upon doping with 0.6 holes/nm, the E_{11} exciton delocalizes over tens of nm along the tube axis (at zero temperature, the envelope function fall-off at large electron-hole separation is algebraic in the doped case, in contrast to the exponential decay in the undoped case) and acquires nodes separated by ~ 5 nm.
 - [18] L.J. Sham and T.M. Rice, *Phys. Rev.* **144**, 708 (1966).
 - [19] H. Schweizer et al., *Phys. Rev. Lett.* **51**, 698 (1983).

- [20] S.I. Gubarev et al., JETP Lett. **76**, 575 (2002).
- [21] In bulk degenerate semiconductors, doping also leads to a blue-shift of the optical absorption edge (the Burstein-Moss effect), but in that case band filling is the largest effect; see E. Burstein, Phys. Rev. **93**, 632 (1954).
- [22] J.U. Lee, Phys. Rev. B **75**, 075409 (2007).